

Noble gas tracers of ventilation during deep-water formation in the Weddell Sea

This content has been downloaded from IOPscience. Please scroll down to see the full text.

2016 IOP Conf. Ser.: Earth Environ. Sci. 35 012019

(<http://iopscience.iop.org/1755-1315/35/1/012019>)

View [the table of contents for this issue](#), or go to the [journal homepage](#) for more

Download details:

IP Address: 163.1.203.194

This content was downloaded on 13/01/2017 at 15:01

Please note that [terms and conditions apply](#).

Noble gas tracers of ventilation during deep-water formation in the Weddell Sea

D P Nicholson¹, S Khatiwala² and P Heimbach^{3,4}

¹Marine Chemistry and Geochemistry Department, Woods Hole Oceanographic Institution, 266 Woods Hole Road, Woods Hole, MA 02543, USA

²Department of Earth Sciences, University of Oxford, South Parks Road, Oxford OX1 3AN, UK

³Institute for Computational Engineering and Sciences & Jackson School of Geosciences, The University of Texas at Austin, 201 East 24th Street, POB 4.232, Austin, TX 78712, USA

⁴Department of Earth, Atmospheric and Planetary Sciences, Massachusetts Institute of Technology, 77 Massachusetts Avenue, Cambridge, MA, 02139, USA

E-mail: dnicholson@whoi.edu

Abstract. To explore the dynamics and implications of incomplete air-sea equilibration during the formation of abyssal water masses, we simulated noble gases in the Estimating the Circulation & Climate of the Ocean (ECCO) global ocean state estimate. A novel computation approach utilizing a matrix-free Newton–Krylov (MFNK) scheme was applied to quickly compute the periodic seasonal solutions for noble gas tracers. MFNK allows for quick computation of a cyclo-stationary solution for tracers (i.e., a spun-up, repeating seasonal cycle), which would otherwise be computationally infeasible due to the long time scale of dynamic adjustment of the abyssal ocean (1000’s of years). A suite of experiments isolates individual processes, including atmospheric pressure effects, the solubility pump and air-sea bubble fluxes. In addition to these modeled processes, a volumetric contribution of $0.28 \pm 0.07\%$ of glacial melt water is required to reconcile deep-water observations in the Weddell Sea. Another primary finding of our work is that the saturation anomaly of heavy noble gases in model simulations is in excess of two-fold more negative than is suggested from Weddell Sea observations. This result suggests that model water masses are insufficiently ventilated prior to subduction and thus there is insufficient communication between atmosphere and ocean at high latitudes. The discrepancy between noble gas observations and ECCO simulations highlights that important inadequacies remain in how we model high-latitude ventilation with large implications for the oceanic uptake and storage of carbon.

1. Introduction

The vast abyssal ocean is ventilated by a few limited surface regions of deep-water formation including the Labrador Sea and Weddell Sea [1]. Thus, ocean storage of dissolved inorganic carbon (DIC) depends critically on air-sea exchange processes in these regions [2–4]. The zonally and vertically integrated poleward volume transport results in the meridional overturning circulation, which is composed of an upper (northern) and lower (southern) cell resulting in upwelling in the

¹ To whom any correspondence should be addressed.



Southern Ocean, a portion of which returns to depth, contributing to Antarctic Bottom Water formation (figure 1). This portion of the flow experiences incomplete ventilation while at the (often sea-ice covered) surface in the Southern Ocean [5]. The degree to which Southern Ocean surface waters equilibrate before subducting to form either AABW or intermediate water masses has a large impact on the efficiency with which preformed nutrients are utilized [6] and the ocean-atmosphere partitioning of CO_2 . The resultant degree of partial equilibration dramatically influences the DIC capacity of the ocean, atmospheric pCO_2 and global climate [3,7].

Noble gases record this incomplete equilibration as evidenced by observed undersaturation of heavy noble gases (Xe, Kr) in the deep ocean [8–10]. While the inorganic carbon system is subject to complex interactions of biological and physical mechanisms, the noble gases are abiotic and thus useful for isolating and understanding the physical dynamics of air-sea gas exchange and ventilation. Here, we combine numerical simulations with noble gas observations to examine signatures of incomplete equilibration in the deep Weddell Sea.

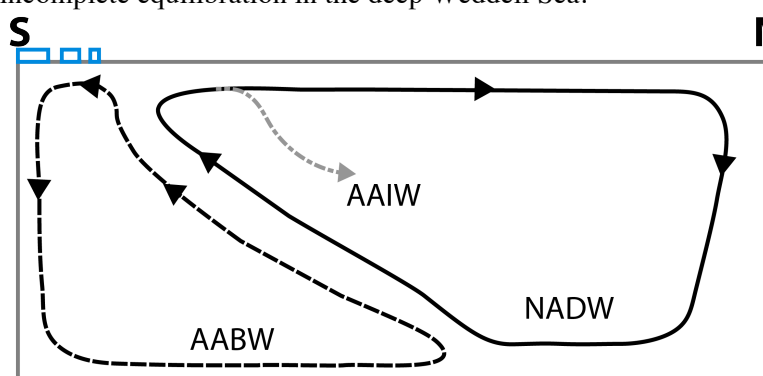


Figure 1. Schematic of the meridional overturning circulation, showing North Atlantic Deep Water (NADW), Antarctic Bottom Water (AABW) and Antarctic Intermediate Water (AAIW). Air-sea equilibration time in the Southern Ocean is limited by residence time, partial sea-ice cover and deep winter mixed layer depths.

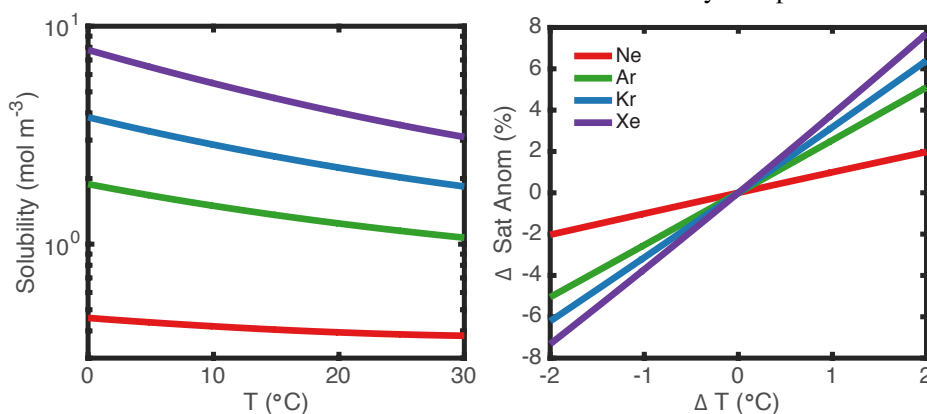


Figure 2. Solubility of noble gases (left) and temperature dependence of solubility at 5°C (right). The right panel shows the resulting change in saturation state given a change in temperature without change in gas concentration.

2. Background

The noble gases are useful tracers of air-sea processes because they have a range of physical properties (figure 2). Each has a well-known boundary condition (a well-mixed tropospheric value) and with the exception of He, they have no sources or sinks in the ocean interior [11]. These tracers have previously been applied to understand a range of oceanic processes, including air-sea bubble fluxes [12,13], diapycnal mixing [14,15], ventilation during deepwater formation [8, 9] and glacial melting [10]. Generally, the concentration of noble gases is within a few percent of solubility equilibrium,

with small deviations induced by a range of physical processes of interest. Fortunately, such saturation anomalies (ΔC) can analytically be determined precisely and are denoted as:

$$\Delta C = \left(\frac{[C] - [C]_{eq}}{[C]_{eq}} \right) \quad (1)$$

where $[C]$ is the measured concentration of gas C , and $[C]_{eq}$ is the temperature and salinity-dependent equilibrium solubility at 1 atm and saturated water vapour pressure [16–18].

The air-sea interface is the dominant source and sink for dissolved noble gases in the ocean. The air-sea flux of sparingly soluble gases such as the noble gases is distinctly influenced by bubble-mediated processes [19–21] and thus an explicit bubble parameterization is warranted. Following previous noble gas studies [12, 13, 22], we parameterize air-sea flux to include a term for the surface diffusive component, as well as two bubble-mediated flux terms such that the net air to sea flux (F_{as}) is:

$$F_{as} = F_{surf} + F_{bub} \quad (2)$$

where:

$$F_{surf} = -k_c(1 - f_{ice})(\delta C^P) \quad (3)$$

where k_c is the diffusive gas transfer velocity (m s^{-1}) and δC^P (mol m^{-3}) is the concentration anomaly corrected for local atmospheric pressure:

$$\delta C^P = [C] - [C]_{eq} \left(\frac{p_{slp} - p_w}{p_{ref} - p_{wsat}} \right) \quad (4)$$

where p_{slp} (atm) is sea level pressure, p_w (atm) is water vapour pressure at the sea surface, p_{ref} (atm) is standard atmospheric pressure, and p_{wsat} (atm) is water vapour pressure at 100% relative humidity,

$$F_{bub} = (1 - f_{ice}) U \chi_C \left(\frac{p_{slp}}{p_{ref}} \right) \left(A_{inj} + A_{ex} \left(\frac{D_C}{D_0} \right)^{0.5} \left(\frac{\alpha_C}{\alpha_0} \right) \right) \quad (5)$$

where $U = ((u_{10} - 2.27)/u_0)^3$ for $u_{10} > 2.27$ and otherwise $U = 0$. A_{inj} and A_{ex} are empirical constants, χ_C is the atmospheric mixing ratio of C , u_{10} is 10-m wind velocity (m s^{-1}), D_C is gas diffusivity ($\text{m}^2 \text{s}^{-1}$) and α_C is gas solubility ($\text{mol m}^{-3} \text{atm}^{-1}$). D_0 , α_0 and u_0 are unit-value normalization constants with values of $1 \text{ m}^2 \text{s}^{-1}$, $1 \text{ mol m}^{-3} \text{atm}^{-1}$ and 1 m s^{-1} , respectively.

2.1. Quasi-steady state

Given a steady wind speed and rate of cooling a surface water parcel will reach a quasi-steady state [14] such that the saturation anomaly is stable (i.e., the above equations are solved for the case where $d(\Delta C^P)/dt = 0$ and $\Delta C^P = \delta C^P/[C]_{eq}$):

$$\Delta C^P = \frac{-H}{c_p k_c (1 - f_{ice}) [C]_{eq}} \frac{d[C]_{eq}}{dT} + \frac{U}{k_c} \left(\frac{p_{slp}}{p_{ref}} \right) \left(\left(\frac{A_{inj}}{\alpha_C} \right) + A_{ex} \left(\frac{D_C}{D_0} \right)^{0.5} \right) \quad (6)$$

where H (W m^{-2}) is air-sea heat flux (positive is heat lost to the atmosphere), c_p ($\text{J m}^{-3} \text{K}^{-1}$) is the heat capacity and T ($^{\circ}\text{C}$) is mixed layer temperature. The above quasi-steady-state equation is composed of a cooling/warming driven anomaly and a bubble-mediated anomaly. The magnitude of the temperature induced surface anomaly is larger for the heavy noble gases (due to larger $d([C]_{eq})/dT$) while the bubble component is smaller for the heavy gases (due to larger α_C). Another notable implication of the above equation is that ice cover amplifies the saturation anomaly due to heating/cooling, but cancels out for bubble-induced anomaly.

The quasi-steady-state framework is useful to illustrate how saturation anomaly is composed of a surface component driven by air-sea heat flux and a bubble-mediated component. Atmospheric pressure, which typically can reach 2–3% below 1 atm at high latitude also contributes to ΔC .

Table 1. Description and units for equation terms

Abbreviation	Description	Units
$[C]$	Dissolved concentration of gas	mol m^{-3}
$[C]_{eq}$	Equilibrium $[C]$ w.r.t. 1 atm and saturating water vapour pressure	mol m^{-3}
ΔC	Gas saturation anomaly	unitless
F_{as}	Total Air-sea gas flux	$\text{mol m}^{-2} \text{s}^{-1}$
F_{surf}	Surface air-sea gas flux	$\text{mol m}^{-2} \text{s}^{-1}$
F_{bub}	Bubble mediated air-sea gas flux	$\text{mol m}^{-2} \text{s}^{-1}$
k_c	Gas transfer piston velocity	m s^{-1}
f_{ice}	Fraction ice cover	unitless
δC^p	Saturation anomaly relative to local atmospheric pressure	mol m^{-3}
p_{slp}	Sea level pressure	atm
p_w	Water vapour pressure	atm
p_{wsat}	Saturation water vapour pressure	atm
χ_C	Dry atmospheric molar mixing ratio	mol/mol
A_{inj}	Emperical constant for bubble injection	$\text{mol m}^{-2} \text{s}^{-1}$
A_{ex}	Emperical constant for bubble exchange	$\text{mol m}^{-2} \text{s}^{-1}$
u_{10}	10-meter wind speed	m s^{-1}
D_C	Gas diffusivity	$\text{m}^2 \text{s}^{-1}$
α_C	Gas solubility	$\text{mol m}^{-3} \text{atm}^{-1}$
H	Net air-sea heat flux (negative for ocean cooling)	W m^{-2}
c_p	Seawater heat capacity	$\text{J m}^{-3} \text{K}^{-1}$
T	seawater temperature	$^{\circ}\text{C}$

3. Model methods

3.1. The noble gases in ECCO

The circulation used in this study is based on an ocean state estimate provided by the Estimating the Circulation & Climate of the Ocean (ECCO) consortium [23]. The ECCO ocean state estimate (ECCO version 2) was achieved by adjusting the air-sea fluxes of heat, momentum and freshwater in the MIT ocean general circulation model [24] through data assimilation [25, 26]. This procedure results in a dynamically consistent estimate of ocean circulation and hydrography over the assimilation period. The model has a horizontal resolution of 1° with 23 vertical levels. The actual tracer simulations were performed using the transport matrix method (TMM), an offline scheme for simulation of ocean biogeochemical tracers [27, 28]. Furthermore, in order to efficiently spin-up each of the large number of runs to equilibrium, a matrix-free Newton–Krylov method was used [29]. This approach is significantly more efficient than simply integrating the model to equilibrium. Monthly mean transport matrices, representing a climatology over the 1992–2004 assimilation period, were extracted from the ECCO state estimate and used to carry out the tracer simulations. The ECCO transport matrices along with the TMM code are available from <https://github.com/samarkhatala/tmm>. Our model solutions are thus comparable to a fully spun-up ocean with a seasonal cycle representative of the average seasonal cycle for the model training period (1992–2004).

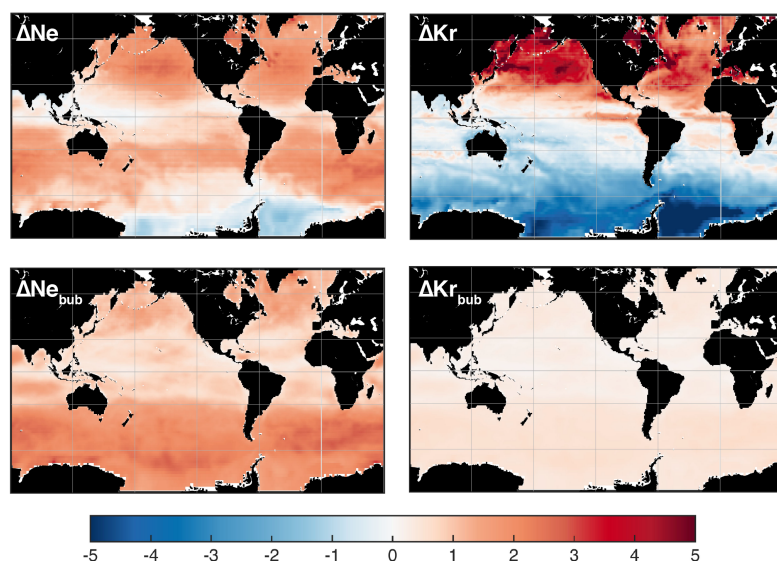


Figure 3. Modelled noble gas surface saturation anomalies shown for July for Ne (left) and Kr (right). Upper panels show total saturation anomaly while lower panels show the anomaly due to air-sea bubble flux. While bubble processes dominate surface ΔNe patterns they have a much smaller impact on ΔKr , which is dictated largely by saturation anomalies due to cooling and warming.

3.2. The noble gases in ECCO

Noble gases were simulated by applying equations (2)–(5) to dictate air-sea exchange. The gas transfer velocity was quadratic with wind speed using the parameterization of Sweeney *et al.* [30], and wind speed and sea level pressure taken from the 6-hourly CORE v2 dataset [31]. Gas diffusivities are calculated from Jahne *et al.* [32] and solubilities for Ne and Ar from Hamme and Emerson [16], for Kr from Weiss and Kyser [17] and for Xe from Wood and Caputi [18] adding a 2% correction as suggested by Hamme and Severinghaus [8].

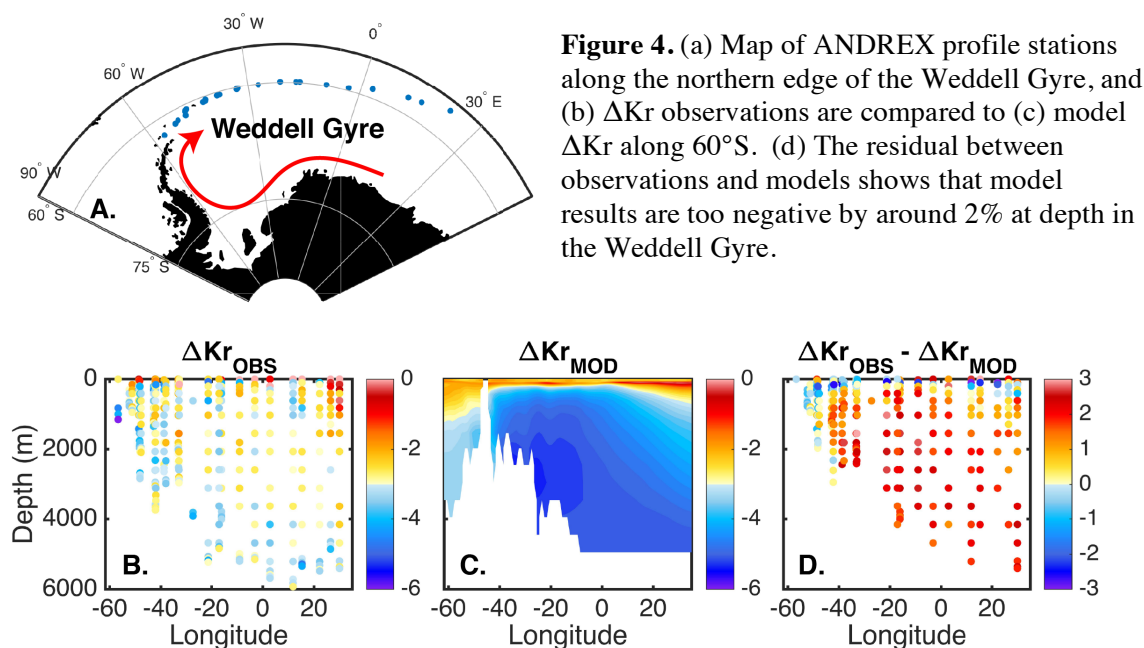
Model simulations allow us to decompose noble gas saturation anomaly into a contribution from each relevant process. To do so, four simulations were performed for each noble gas consisting of (sim1) diffusive gas exchange only (A_{ex} and $A_{inj} = 0$), (sim2) diffusive gas exchange plus bubble injection ($A_{ex} = 0$), (sim3) diffusive gas exchange plus bubble exchange ($A_{inj} = 0$), and (sim4) all processes ‘on’. Saturation anomaly due to a single process is calculated from the difference of two simulations, for example, $\Delta Ne_{inj} \approx \Delta Ne_{sim4} - \Delta Ne_{sim2}$ (figure 3).

4. Results

4.1. Air-sea bubble fluxes and atmospheric pressure

Similar to our previous work [13], but using a seasonally resolving and higher spatial resolution model, we constrained the magnitude of bubble injection and bubble exchange terms, A_{inj} and A_{ex} . All available Ne, Ar, Kr, Xe and N_2 observations from below 500 m were used in the inverse calculation. Best-fit values were $A_{inj} = 1.06 \times 10^{-9}$ and $A_{ex} = 2.19 \times 10^{-6}$. These values are 37% and 71% lower than previously published values for A_{inj} and A_{ex} , respectively [13]. Improvements in the underlying model, as well as the addition of newly published data contribute to the difference, but the primary cause for a lower bubble flux estimate is the use of higher-frequency wind forcing. In prior methods, monthly average winds were used and Rayleigh wind speed distributions were assumed to correct for non-linear averaging effects. In the current study, necessary non-linear wind speed forcing quantities ($u_{10} - 2.27$)³ and u_{10}^2 were calculated using 6-hourly winds, obviating the need for assumptions about wind speed distributions.

Beyond refining estimates of air-sea bubble fluxes, we constrain bubble fluxes here in order to remove the bubble signal from heavy noble gas distributions and focus on cooling driven undersaturation of the heavy noble gases. We find that for Kr and Xe, air sea bubble fluxes are a relatively minor component of observed saturation anomaly, contributing less than 1% saturation anomaly (figure 4). In the deep Weddell Sea, the combination of the two bubble mechanisms increase saturation anomalies for Ne, Ar, Kr and Xe by 2.1%, 0.7%, 0.5% and 0.3%, respectively. Consistently



low atmospheric pressure around the Antarctic continent reduces the saturation anomaly for each gas by 1.6%.

4.2. Comparison to Weddell Sea observations

A recently published dataset [10] provides the first comprehensive observations that include the heavy noble gases in the Southern Ocean. The data were collected in April 2010 as part of the Antarctic Deep Water Rates of Export (ANDREX) project and consist of a quasi-zonal section through the Weddell gyre, approximately along the 60°S parallel from near the Drake Passage at 60°W to 30°E (figure 4). At the surface, there is significant seasonality in modelled gas saturation anomaly (supplementary figure S1) and observations are noisier, likely due to short term variability on time-scales shorter than the monthly-mean model results (figures S1 and 4). Compared to ANDREX observations the deep Weddell gyre is significantly more undersaturated in the model. For a light noble gas modelled ΔNe also was significantly lower than observations. We identify that these discrepancies are due to deficiencies in two processes: (1) The model does not include a contribution from glacial meltwater (GMW) and (2) the surface cooling driven anomaly (ΔC_{surf}) appears to be too large in the model.

In the Southern Ocean, the addition of noble gases from glacial ice shelves contributes a source of dissolved noble gases not considered in our model. Glacial ice contains significant air content trapped in bubbles with a unique noble gas signature, as noble gas saturation anomalies are altered from atmospheric abundance by differential diffusion, gravitational enrichment and bubble processes [33]. Basal melting of glacial ice results in the addition of a distinct source of dissolved noble gases with the net effect of significantly increasing the saturation anomaly of the lighter gases and slightly decreasing

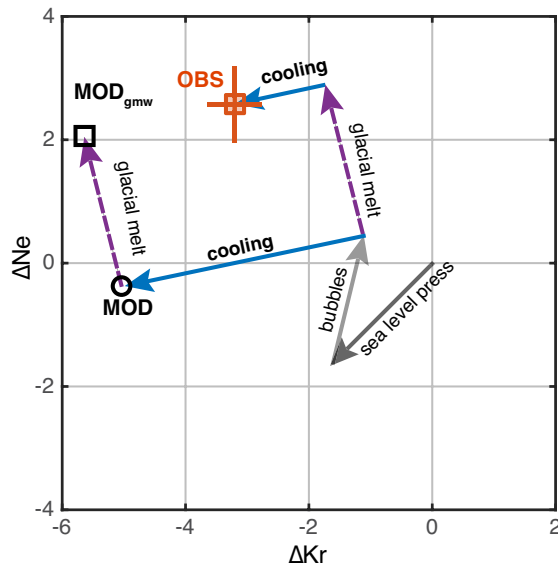


Figure 5. Model solution for the deep Weddell Sea (depth > 3500 m) is shown in Kr vs. Ne space. Results from ECCO (MOD) are shown with a black circle. After adding the glacial meltwater correction, modelled anomalies are located at the black square (MOD_{gmw}). Observations are indicated by the orange rectangle with 1 standard deviation error bars. The magnitude of cooling-driven saturation anomaly needed to reach MOD_{gmw} is over twice that needed to reach OBS.

the saturation anomaly of heavier noble gases such that $\Delta\text{Ne}_{\text{gmw}} = 8.9\%$, $\Delta\text{Ar}_{\text{gmw}} = -0.5\%$, $\Delta\text{Kr}_{\text{gmw}} = -2.2\%$ and $\Delta\text{Xe}_{\text{gmw}} = -3.3\%$ per 1% volumetric contribution of GMW [10].

The cooling coupled with incomplete equilibration (the solubility pump) results in a saturation anomaly proportional to $D_c^{0.5} \left(1/[C]_{eq} \right) d[C]_{eq}/dT$ such that the heavy noble gases with slower diffusivity (D) and greater temperature dependence of solubility sustain a greater cooling-driven undersaturation (ΔC_{surf}). Thus, the sensitivity of Kr to cooling is much greater than that of Ne such that $\Delta\text{Kr}_{\text{surf}} / \Delta\text{Ne}_{\text{surf}} \approx 5.0$.

Equations for two gases, Ne and Kr, can be solved for the ΔC_{surf} and f_{gmw} needed to achieve the observed anomaly in the deep Weddell Sea ($\Delta\text{Ne} = 2.6 \pm 0.6\%$, $\Delta\text{Kr} = -3.2 \pm 0.4\%$) [10]. The solution is shown graphically in figure 5. Our solution yields an estimated f_{gmw} of $0.28 \pm 0.07\%$ in the deep Weddell Sea. Adding this correction factor to model results increases ΔNe by 2.4% and decreases ΔKr and ΔXe by 0.6% and 0.9%, respectively. The magnitude of cooling required to match observations was $\Delta\text{Ne}_{\text{surf}} = -0.3\%$ and $\Delta\text{Kr}_{\text{surf}} = -1.5\%$. This observationally constrained cooling anomaly was much less than the cooling anomaly calculated directly by the model of $\Delta\text{Ne}_{\text{surf}} = -0.8\%$ and $\Delta\text{Kr}_{\text{surf}} = -3.8\%$. Ne and Kr are an ideal pair for constraining these processes as the impact of these processes are nearly orthogonal in ΔKr vs. ΔNe space (figure 5). Similar results are obtained with other pairs of gases.

5. Discussion

The saturation anomaly in the abyssal deep Weddell Sea is composed of contributions from atmospheric pressure variation, air-sea bubble flux, glacial meltwater and the cooling-driven solubility pump. Here, we combine modelling and observations to estimate the contribution of glacial meltwater and the solubility pump. Noble gas constraints suggest a contribution of $0.28 \pm 0.07\%$ glacial meltwater to the deep Weddell Sea along the ANDREX section (figure 4).

Additionally, we identify a discrepancy between model and observations for the heavy noble gases that we attribute to an overly inefficient solubility pump in the ECCO-based model simulation. For the model the solubility pump component results in a $\Delta\text{Kr}_{\text{surf}} = -3.8\%$, while observations suggest that $\Delta\text{Kr}_{\text{surf}} = -1.5\%$ is more realistic (figure 5).

From equation (6) we see that in addition to physical properties of the noble gases, the magnitude of cooling-driven saturation anomaly scales proportionally with $-H/k(1-f_{\text{ice}})$. Thus we consider air-sea heat flux and the diffusive gas exchange rate as the likely sources of deficiency in the model simulations. A cooling flux of too great magnitude could be indicative of the tendency of 1° global

models to create Southern Ocean deep water via open ocean convection, rather than shelf processes [34]. The regions where the deep Weddell Gyre was ventilated are shown in supplementary figure S2. Given the relatively high ice-cover in the Weddell Sea, a bias in the ice inhibition of air-sea transfer term, $(1-f_{ice})$, could have a large impact on the solubility pump as well. We note that sea ice and abyssal water formation through density currents are both particularly challenging problems for most earth system models including ECCO [34–36].

Whatever the cause, insufficient ventilation at the time and location of deepwater formation will have large implications for the global biogeochemical cycles of carbon and a range of dissolved gases. Noble gas tracers indicate that model deepwater retains a cooling-induced saturation anomaly that is over twice what observations suggest it should be. Such model shortcomings might be expected to result in underestimation of the uptake of anthropogenic carbon and transient tracers in the Southern Ocean. Our analysis suggests the promise of noble gas tracers as an independent way of assessing the fidelity of ocean circulation models (and state estimates). The future availability of TMM matrices for a range of models and model configurations will enable an efficient framework for such an assessment.

References

- [1] Broecker W S and Peng T 1982 *Tracers in the Sea* (Palisades, New York: Lamont-Doherty Geological Observatory, Columbia University)
- [2] Toggweiler J R and Sarmiento J L 1985 Glacial to interglacial changes in atmospheric carbon dioxide: The critical role of ocean surface water in high latitudes *The Carbon Cycle and Atmospheric CO₂: Natural Variations Archean to Present* eds E T Sundquist and W S Broecker (Washington, DC: American Geophysical Union)
- [3] Toggweiler J R *et al* 2003 *Glob. Biogeochem. Cycles* **17** 1026
- [4] Maier-Reimer E and Hasselmann K 1987 *Clim. Dyn.* **2** 63
- [5] Jones D C *et al* 2014 *Glob. Biogeochem. Cycles* **28** 1163
- [6] Marinov I *et al* 2006 *Nature* **441** 964
- [7] Ferrari R *et al* 2014 *Proc. Natl. Acad. Sci.* **111** 8753
- [8] Hamme R C and Severinghaus J P 2007 *Deep-Sea Res. Part I* **54** 939
- [9] Nicholson D *et al* 2010 *J. Geophys. Res. Oceans* **115** C11015
- [10] Loose B and Jenkins W J 2014 *Geophys. Res. Lett.* **41** 2013GL058804
- [11] Stanley R H R and Jenkins W J 2013 Noble Gases in seawater as tracers for physical and biogeochemical ocean processes *The Noble Gases as Geochemical Tracers Advances in Isotope Geochemistry* ed P Burnard (Springer Berlin Heidelberg) 55–79
- [12] Stanley R H R *et al* 2009 *J. Geophys. Res. Oceans* **114** C11020
- [13] Nicholson D, *et al* 2011 An inverse approach to estimate bubble-mediated air-sea gas flux from inert gas measurements *Proceeding of the 6th international symposium on gas transfer at water surfaces* (Kyoto, Japan: Kyoto University Press)
- [14] Ito T and Deutsch C 2006 *Glob. Biogeochem. Cycles* **20** GB3019
- [15] Emerson S *et al* 2012 *Geophys. Res. Lett.* **39** L18610
- [16] Hamme R C and Emerson S R 2004 *Deep-Sea Res. Part I* **51** 1517
- [17] Weiss R F and Kyser T K 1978 *J. Chem. Eng. Data* **23** 69
- [18] Wood D and Caputi R 1966 *Solubilities of Kr and Xe in fresh and sea water* USNRDL TR 988 (San Francisco, CA: US Naval Radiological Defense Laboratory)
- [19] Keeling R F 1993 *J. Mar. Res.* **51** 237
- [20] Fuchs G *et al* 1987 *J. Geophys. Res.-Oceans* **92** 6559
- [21] Jenkins W J *et al* 1988 *Philos. Trans. R. Soc. Lond. Ser. Math. Phys. Sci.* **325** 43
- [22] Hamme R C and Emerson S R 2006 *J. Mar. Res.* **64** 73
- [23] Wunsch C *et al* 2009 *Oceanography* **22** 88
- [24] Adcroft A *et al* 2004 Overview of the formulation and numerics of the MIT GCM *Proceedings of the ECMWF Seminar on “Recent developments in numerical methods for atmospheric*

- and ocean modelling*” (Shinfield Park, Reading, UK) 139–50
- [25] Wunsch C and Heimbach P 2007 *Phys. Nonlinear Phenom.* **230** 197
- [26] Wunsch C and Heimbach P 2013 Dynamically and kinematically consistent global ocean circulation and ice state estimates *Ocean Circulation and Climate: A 21st Century Perspective* eds G Siedler *et al* (Academic Press) 553–79
- [27] Khatiwala S *et al* 2005 *Ocean Model.* **9** 51
- [28] Khatiwala S 2007 *Glob. Biogeochem. Cycles* **21** doi:10.1029/2007GB002923
- [29] Khatiwala S 2008 *Ocean Model.* **23** 121
- [30] Sweeney C *et al* 2007 *Glob. Biogeochem. Cycles* **21** doi:10.1029/2006GB002784
- [31] Large W G and Yeager S G 2008 *Clim. Dyn.* **33** 341
- [32] Jähne B *et al* 1987 *J. Geophys. Res.* **92** 10767
- [33] Severinghaus J P and Battle M O 2006 *Earth Planet. Sci. Lett.* **244** 474
- [34] Heuzé C *et al* 2013 *Geophys. Res. Lett.* **40** 1409
- [35] Legg S *et al* 2009 *Bull. Am. Meteorol. Soc.* **90** 657
- [36] Turner J *et al* 2012 *J. Clim.* **26** 1473

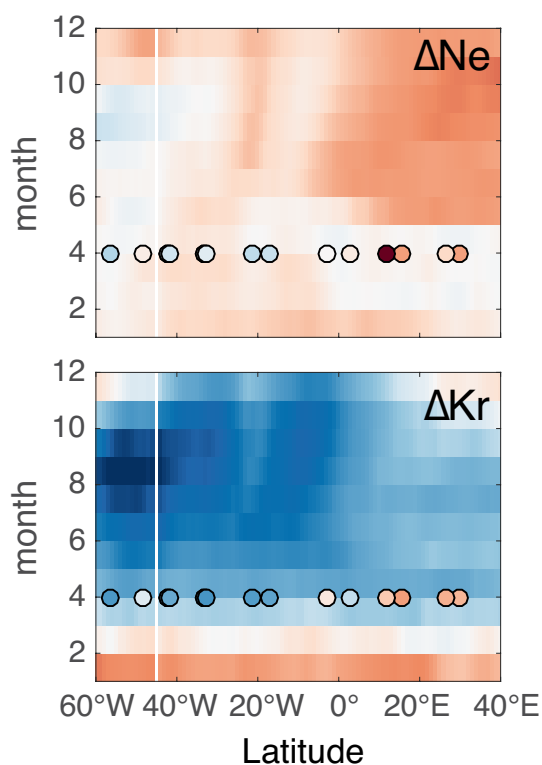


Figure S1. Hovmöller diagram of monthly mean surface ΔNe and ΔKr along 60°S with ANDREX observations from April 2010 overlaid.

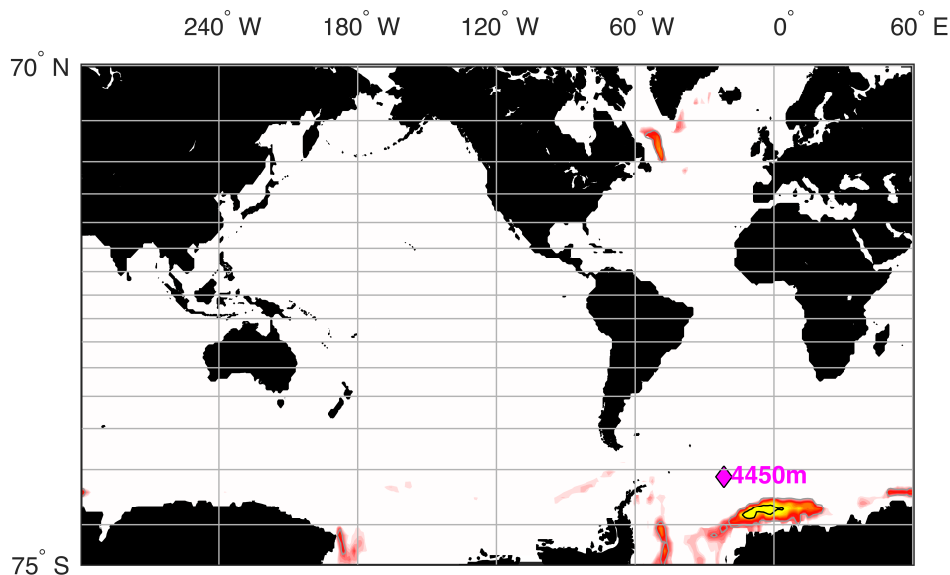


Figure S2. Results for an adjoint Green function calculation for a target volume in the deep Weddell Gyre (21.3°W 61.6°S at 4450 m) was last ventilated. The pink marker indicates the location of the deep (4450 m) target volume. The solid black contour encloses a region accounting for where 50% of the water parcel was ventilated and the light grey contour encloses where 90% of ventilation occurred.